ADA078663

AFGL-TR-79-0191
ENVIRONMENTAL RESEARCH PAPERS, NO. 672

LEVEL

Absorption Data Analysis for EUVS Experiment on the Satellites AE - C, D, and E
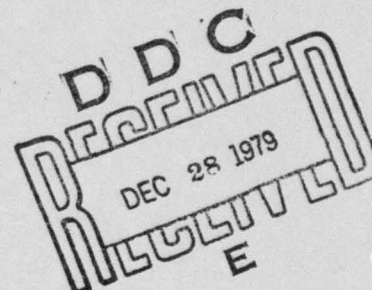
LES M. CHAIKIN
KATSURA FUKUI

8 August 1979

DDC
RECEIVED
DEC 28 1979
E

DDC FILE COPY

AERONOMY DIVISION   PROJECT 6690
AIR FORCE GEOPHYSICS LABORATORY
HANSCOM AFB, MASSACHUSETTS 01731
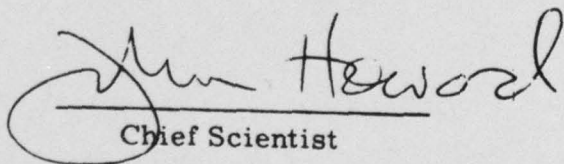
AIR FORCE SYSTEMS COMMAND, USAF

79-12 27 292

This report has been reviewed by the ESD Information Office (OI) and is releasable to the National Technical Information Service (NTIS).

This technical report has been reviewed and is approved for publication.

FOR THE COMMANDER

Chief Scientist

REPORT DOCUMENTATION PAGE	READ INSTRUCTIONS BEFORE COMPLETING FORM

1. REPORT NUMBER	2. GOVT ACCESSION NO.	3. RECIPIENT'S CATALOG NUMBER
AFGL-TR-79-0191	AFGL-ERP-672	

4. TITLE (and Subtitle)	5. TYPE OF REPORT & PERIOD COVERED
ABSORPTION DATA ANALYSIS FOR EUVS EXPERIMENT ON THE SATELLITES AE-C, D, and E	Scientific. Interim.
	6. PERFORMING ORG. REPORT NUMBER
	ERP No. 672

7. AUTHOR(s)	8. CONTRACT OR GRANT NUMBER(s)
Les M. Chaikin Katsura Fukui	

9. PERFORMING ORGANIZATION NAME AND ADDRESS	10. PROGRAM ELEMENT, PROJECT, TASK AREA & WORK UNIT NUMBERS
Air Force Geophysics Laboratory Hanscom AFB Massachusetts 01731	62101F 66901602

11. CONTROLLING OFFICE NAME AND ADDRESS	12. REPORT DATE
Air Force Geophysics Laboratory Hanscom AFB Massachusetts 01731	8 Aug 1979
	13. NUMBER OF PAGES
	48

14. MONITORING AGENCY NAME & ADDRESS(if different from Controlling Office)	15. SECURITY CLASS. (of this report)
	Unclassified
	15a. DECLASSIFICATION/DOWNGRADING SCHEDULE

16. DISTRIBUTION STATEMENT (of this Report)

Approved for public release; distribution unlimited.

17. DISTRIBUTION STATEMENT (of the abstract entered in Block 20, if different from Report)

19. KEY WORDS (Continue on reverse side if necessary and identify by block number)

Absorption
EUVS
Satellite

20. ABSTRACT (Continue on reverse side if necessary and identify by block number)
One of the two tasks that the Extreme Ultraviolet Spectrophotometers (EUVS) onboard the Atmosphere Explorer Satellites perform is absorption analysis of the thermosphere. The optical depth is derived from observations during parts of orbits including conditions of nearly negligible attenuation as reference. Details of two different approaches are described. The first one, used by the program LMC80, deals with certain standard optical depths only; the second one, used by the program LMC85, deals with time-ordered records of optical depths for input-controlled fixed steps in time.

409 578

Contents

3

Illustrations

Tables

4

Absorption Data Analysis for EUVS Experiment
on the Satellites AE-C, D, and E

1. INTRODUCTION

The purpose of the Extreme Ultraviolet Spectrophotometer (EUVS) absorption analysis system is to determine quantitative characteristics of the thermosphere (95-400 km) including the diurnal, seasonal, and latitudinal variations of these characteristics. Results on particle-number densities of nitrogen and oxygen (N_2, O and O_2), temperature, total mass density, and scale height have been obtained for various atmospheric regions. Other studies in the future will include the distribution of vibrational states of molecular oxygen and the spatial and temporal variations of this distribution.

The EUVS instruments take data onboard the Atmosphere Explorer (AE) satellites and each consists of 24 monochromators which are held in a biaxial gimbal device that can be pointed at the target position on the solar disk commanded by the experimenter. Twelve of these monochromators, MN Nos. 1 through 12, are scan-capable, that is, they can scan a range of wavelengths. Most of these, that is, all except MN Nos. 11 and 12, have full-disk view of the sun and are primarily used for the EUVS solar flux analysis. The remaining 12 monochromators, MN Nos. 13 through 24, are fixed at specific wavelengths of aeronomical interest and have a narrower field-of-view. They are used primarily for the absorption analysis. A detailed description was published elsewhere.[1]

1. Hinteregger, H. E., Bedo, D. E., and Manson, J. E. (1973) The EUV spectrophotometer on Atmosphere Explorer, Radio Science 8(No. 4):349-359.

2. RESULTS OF EUVS ABSORPTION DATA ANALYSIS

Absorption results from EUVS fall into two categories. The first covers results based only on observations from EUVS. These are the optical depths, τ, derived at each wavelength from the observed signals by the relation

$$S = S_o e^{-\tau} \tag{1}$$

where S is the observed flux and S_o is the incident unattenuated flux. These optical depths are obviously independent of any model assumptions on absorption cross sections and provide the best means of comparing any model prediction with the actual observations of EUVS.

The second category of results are those which are based on these optical depth data, but do involve the knowledge of absorption cross sections and certain assumptions of atmospheric models. These results include the aeronomical parameters such as particle-number densities and temperatures. While the results of this second category may be of more direct interest to aeronomy, they obviously involve the adoption of certain model concepts and specific reference data required to produce them. The algorithms which produce both types of data will be discussed here, along with an analysis of the types of error encountered and the data currently available.

Telemetry data of EUVS observations come in the form of 8-sec blocks (or so-called major frames of 128 minor frames of 1/16 sec each). Each of these blocks contains 16 data groups spaced 0.5 sec apart (8 minor frames). The latter 0.5-sec groups are called "EUVS frames." The monochromators are assembled in pairs and each pair ("module") shares a common detector (either a chenneltron or photomultiplier tube). This means that only one of the monochromators of a given module can be sampling solar radiation in any given 0.5-sec interval. Therefore, each of the 16 EUVS frames of one major frame contains not only the count samples from each of the 12 detectors, but also the aperture-exposure index along with the grating step positions and other instrumental parameters needed for a complete identification of the EUVS data received.

Absorption analysis deals with the observations taken at 20 selected wavelengths of aeronomical interest. A listing of those 20 wavelengths and the reference data on absorption cross section selected for the production of density data for the vehicle AE-C are given in Table 1 as an example, where LL = 1-20 serves as the identification number. The column ANG gives the wavelength (λ) for each LL number in Å units. All 20 wavelengths are the same for all three EUV instruments (on AE-C, D, and E) with the exception of LL = 13 which represents λ = 610 Å for AE-C, but 304 Å for AE-D and E. Details of the reference data will be discussed in Section 3.2. Due

6

to the aperture and step positions corresponding to the instrumental realization of observations at these selected wavelengths, only eight may be sampled in any given 0.5-sec interval. The overwhelming part of the existing EUVS absorption data reflects observations during experiment turn-ons (passes) with apertures left in a fixed position. Therefore only 8 of the 20 wavelengths are generally present in a given pass. For part of the early life of the AE-C EUVS instrument, the apertures were alternated periodically, and consequently, each 1-sec period of two contiguous EUVS frames contains 16 wavelengths in the data for a given pass. Each wavelength is then, of course, covered with a time resolution of 1.0 sec (instead of 0.5 sec).

Table 1. Twenty Wavelengths and the Reference Data for AE-C

LL	ANG	BREF	SOREF	IULIM	ILLIM	HQHIREF	HQLOWREF	SCALEHTREF	SENSITIVITY
1	175	1.5	460	2400	0	481	306	38	1
2	465	1.5	50	800	0	527	352	47	1
3	584	0.5	2100	6000	0	550	375	47	1
4	765	80.0	1000	30,000	0	500	330	38	1
5	855	50.0	400	9000	50	490	320	47	1
6	1609	128.0	3800	5000	50	260	184	17	2
7	1457	110.0	950	1400	50	280	204	18	1
8	1700	120.0	6600	9000	50	230	155	16	2
9	1730	110.0	9200	11,000	50	215	140	16	2
10	1835	8.0	10,100	12,000	50	160	115	11	2
11	256	2.0	80	500	0	520	345	42	1
12	304	2.5	75	500	0	540	355	46	1
13	610	2.8	81	500	0	550	375	47	1
14	465	26.0	450	4000	0	527	352	47	1
15	584	37.0	210	800	0	550	375	47	1
16	1026	25.0	700	2600	10	235	159	15	2
17	977	25.0	600	2600	10	270	210	18	1
18	1216	0.0	100	500	0	160	115	11	2
19	1600	85.0	3320	6000	50	260	184	18	2
20	1775	80.0	2330	5000	50	180	125	12	2

Additional words in each EUVS frame are devoted to the solar pointing status of the EUVS instrument and to housekeeping information such as the high-voltage levels. The EUVS absorption analysis system checks the solar pointing status words and deletes from consideration major frames of data taken when the satellite was in the dark or when the sun was not fully acquired. It also checks the point on the solar disk which is under observation to ensure that the instrument is pointing where commanded. Pointing was directed to the center of the solar disk for all AE-D and AE-E geophysical observations by the EUVS instruments. For AE-C, central-pointing

7

was used only until orbit 860. After orbit 860 the pointing target was kept 7 arc min off center. This was done to bring the average alignment of the actual target points of the most important monochromators closer to the true center of the solar disk.

Another point deserves mention here. The EUVS instrument on AE-C experienced severe hardware problems with aperture masking and grating stepping which have been reported by Hinteregger et al.[2] While these problems have had a serious effect upon the flux analysis, the absorption analysis was virtually unaffected, since it does not require absolute fluxes.

3. PRODUCTION OF OPTICAL DEPTH DATA (LMC80)

3.1 Introduction

The EUVS instrument provides direct counts of the solar flux simultaneously for a group of 8 out of the 20 fixed wavelengths selected for analysis. In order to prepare the raw data for use in the physical equations, an "unattenuated" reference signal must be computed and the count samples corrected for background and filtered to eliminate aberrant data such as those due to bad transmission. The data are smoothed to improve the statistical significance and are associated with a quantitative measure of data quality. Upon performance of these functions a data base of the resulting optical depth data is created and upgraded regularly as new telemetry becomes available. The resulting data files contain the dates and times for 16 reference values of optical depth shown in Table 2. These dates and times can be used to obtain all associated orbit and solar ephemeris data needed to characterize the absorption profile of the entire pass.

Table 2. Sixteen Standard Optical Depth Points (τ_{REF})

Low Attenuation Region	Medium Attenuation Region	High Attenuation Region
0.033	0.350	1.750
0.067	0.667	2.000
0.100	1.000	2.500
0.150	1.250	3.000
0.200	1.500	4.500
0.250		

2. Hinteregger, H. E., and Chaikin, L. M. (1977) EUV absorption analysis of thermospheric structure from AE-Satellite observations of 1974-1976, COSPAR Space Research 17:525-532.

The first step of data reduction is to obtain an "unattenuated" reference signal, called S_o.

The data are scanned for an interval where attenuation is negligible. The reference signal is then computed within this interval and is corrected for background. The background corrected reference signal is then used for all subsequent computations of optical depths. Once S_o has been obtained the data are sequentially processed either in the forward or reverse time direction. Each major frame is read, the signals corrected for background and converted to optical depths by Eq. (1), that is,

$$\tau = - \ln(S/S_o) \tag{2}$$

where S is the background-corrected signal. These optical depth data are fitted to curves of the form given by Eq. (7), given later, where Δt is the time interval measured from the start of each fit. The range in time over which the curve fit is applied is varied to obtain a good signal-to-noise ratio and generally covers a time period in which the remote probing point covers a vertical distance corresponding to a scale height or less. This regression provides the data smoothing required to filter out purely statistical variability. The range of the fit is searched for the occurrence of a standard optical depth value. If one is found, the function is inverted, and the time corresponding to it is obtained and stored in the data file. The file also includes the fitting coefficients that allow calculation of optical depths and the standard error as a measure of data quality. The resulting data files can be accessed by a computer program (LMC82) which associates the optical depths with the corresponding orbit and solar ephemeris data.

3.2 Reference Signal Computation and Background Correction

3.2.1 THE SELECTION OF "S_o-ELIGIBLE REGIONS"

The unattenuated reference signal (S_o) can be obtained from the raw data of the satellite pass in several ways differing mainly in how "unattenuated" is defined. The values of S_o are computed separately from each wavelength, and each wavelength may require a different method of computation.

The first and most common method selects timespans for "regions" of the pass so as to meet certain criteria involving altitude, solar zenith angle, and wavelength peculiar absorption characteristics included in the reference data (see Table 1). For these S_o-eligible regions, the reference signals, S_o, are then determined from data within these timespans; the exact method of this reduction is described in the next section. The so-called minimum-ray height or height of the remote probing point (h_Q), illustrated in Figure 1, is accessed once every 8 sec (at the major frame

9

start time) and tested against minimum values of altitude to determine if it is within the unattenuated region. This height must also be below a specified maximum altitude to avoid signal contamination by energetic particles. This maximum is specified in common for all wavelengths because particle contamination is solely a function of the satellite height. The value of this maximum satellite height is an input parameter and can be changed for each pass. In practice, the particle problem was treated by appropriate selection of S_o-eligible regions at sufficiently low satellite heights. The minimum value of h_Q allowable for determination of S_o is different for each wavelength and depends upon both the solar zenith angle and the specific residual attenuation defined as negligible (for example $\tau_R = 0.005$). For this purpose, three reference parameters are associated with each wavelength. These parameters are denoted as HQHIREF, HQLOWREF and SCALEHTREF in Table 1 corresponding to the notation of $h_{Q, 95}$, $h_{Q, 0}$, and H respectively, in the text below.
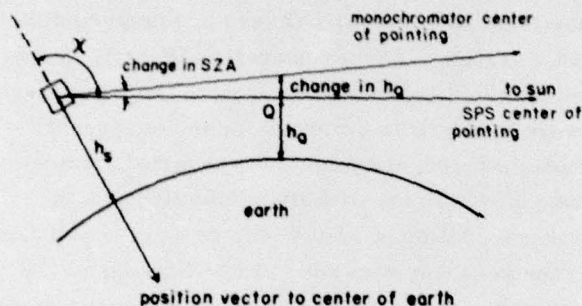
Figure 1. Definitions of Various Quantities

The first of the above is the lowest acceptable altitude for solar zenith angles greater than 95°, the second quantity is the lower limit of altitude for overhead sun where the column mass density is a minimum, and the third quantity is nominal scale height used to calculate the altitude limits for any given zenith intermediary angles. For angles less than arccos (0. 1), the so called "sec χ-approximation" of the optical depth factor is used, that is, calculating

$$h_{Q, \chi} = h_{Q, 0} + H \ln \sec \chi \tag{3}$$

where $h_{Q, \chi}$ is the minimum of h_Q for the given solar zenith angle χ, $h_{Q, 0}$ the value for $\chi = 0$ overhead, and H is the aforementioned scale height parameter. The value of h_Q for zenith angles between arccos (0. 1) and 95° is simply approximated by a linear interpolation between the values for $\chi = 95°$ and the values for $\chi = $ arccos (0. 1), respectively. The specific values of HQHIREF ($h_{Q, 95}$), HQLOWREF ($h_{Q, 0}$) and

10

SCALEHTREF (H) shown in Table 1 for each wavelength reflect the acceptance of a residual optical depth of $\tau_R \leq 0.005$. The values of these three parameters can be modified in accordance with any input value of τ_R other then the most commonly used value of 0.005. In this case the program calculated a corresponding change in the acceptable value of h_Q in the form of

$$\Delta h_Q = -H \ln(\tau_R/0.005) \tag{4}$$

where τ_R is the selected value of accepted residual optical depth. For most of the eccentric orbital phases of AE-C, D, and E, a value of $\tau_R = 0.005$ was used. However, for the subsequent near-circular orbits, the value of τ_R was raised to 0.015 to increase the rate of data return. The actual value of τ_R is carried into the resulting data file.

Depending on orbital characteristics as well as placement and duration of experiment turn-ons on the AE satellites, the number of S_o-eligible regions ranged from none to two per pass. When two S_o-eligible regions do occur within a given turn-on, the corresponding data pass was called "double pass." The data reduction system can seek either one or two S_o-eligible regions for each wavelength separately, or the experimenter can manually enter the regions defined as unattenuated for any selected wavelengths. In the latter case, the system will then accept these regions without executing the aforementioned calculation of a minimum acceptable value of h_Q.

When AE-C and AE-E went into circular orbits at relatively low altitude (~250 km), data on many of the strongly attenuated wavelengths were lost due to the lack of truly unattenuated S_o-eligible regions. To improve the rate of data return over timespans of aeronomical interest, the method of direct input of the timespan for determination of S_o then had to be used frequently. The S_o values so derived were of course not truly unattenuated but reflect actual optical depths ranging up to 0.3 for the worst cases. These values of S_o could be corrected later by a different section of the data reduction system by calculating the residual optical depth for the time of the S_o observations, $\tau_R(S_o)$, to a degree of accuracy considered quite adequate in view of the relatively small magnitudes of $\tau_R(S_o)$ for most wavelengths.

In some rare instances, the experimenter entered actual S_o values directly instead of merely selecting the timespan for which S_o would then be determined by the program.

Regardless of how timespans of S_o-eligible regions are determined, the actual existing measurements are screened for insufficient data. For instance, regions having an insufficient amount of TM data are rejected. This rejection threshold is an input parameter that was normally set to require a minimum of one major frame (8 sec). It should be noted that S_o values are not taken from the whole S_o-eligible

11

region whenever the latter is very large. The maximum size of that part of S_o-eligible regions for which S_o is actually calculated, represents another input parameter (routinely left at five major frames for data production). When it was desired to avoid significant backgrounds by energetic particle fluxes during the period of satellite orbits with high apogee altitudes, the actually used sections of large S_o-eligible regions was selected to be as close to earth as possible. Alternatively, where particle contamination is not a problem, for example, during the phase of circular orbits with altitudes below 400 km, the instructions were switched to select the highest part of the S_o-eligible region. In the routine data production, each of these two options was used where it would give the best results, an identification of this option was carried into the resulting data file.

3.2.2 THE RAW SIGNALS IN S_o-ELIGIBLE REGIONS

All of the data points within the selected section of an S_o-eligible region are input to a standard least square linear regression. The independent variable is the time elapsed in seconds (measured from the start of the selected section). Cramer's rule has been used to solve the resulting two equations for two unknowns. Singular values were identified by a comparison of the absolute value of the determinant with a minimum value. This tolerance is an input parameter which was set at 1.0×10^{-15} for routine data production. Additionally, another input parameter defined the *minimum number of points* for which an S_o determination is considered successful. This parameter was set at six. Data fits having too few points or singular determinants were rejected, and further processing for that wavelength was then omitted.

For successful regressions, the fitted value of the raw signal, $R_o(S_o)$, was then extracted for the center of the fitting interval. The change in signal over the whole S_o-fit range is a measure of the quality of S_o and is, therefore, included in the data file records. Ideally, it should be zero.

To protect the results from contamination by abberrant data, some form of data filtering for the raw signal computation is obviously required. This is accomplished by comparison with fixed upper and lower limits given as reference data for each wavelength. These are set to take a wide range of values, and are essentially designed to filter out transmission errors, stuck bit errors, and so on. The values for these limits are in Table 1 (see quantities called IULIM and ILLIM). Once the raw signal (R_o) is computed, the background is subtracted and the unattenuated reference signal is given as $S_o = R_o - B$.

3.2.3 THE BACKGROUND CORRECTION

A correction for scattered-light background is accomplished by the subtraction $S_o = R_o - B$, where B is determined by a reference value of B_{REF} stated for a reference value of $S_o = S_{o, REF}$. For a given value of R_o, the corresponding background is scaled appropriately, that is,

12

$$B = B_{REF} \, R_o / (S_{o, REF} + B_{REF}) \tag{5}$$

where B_{REF} and $S_{o, REF}$ are listed for each wavelength in Table 1 (denoted as BREF and SOREF respectively). Changes in instrumental sensitivies were caused by the changing detector responses and occasional stepping-up of the operational high voltage. The latter was undertaken to compensate for degradation of pulse-height distributions. Since the optical depth data are generated by taking ratios of the signals, $\tau = \ln(S_o/S)$, the absorption analysis is obviously not sensitive to long-term variation of the absolute photometric sensitivities.

3.2.4   FINAL COMPUTATION OF S_o

The final value of the unattenuated reference signal is computed by subtracting the scaled background from the computed raw signal as shown in Eq. (5). For single passes (satellite data passes containing only one S_o-eligible region) this is the S_o value used for all optical depth computations for that pass. In double passes, where two slightly different reference signals are obtained for two parts of the pass, the final S_o used for the optical depth computation is obtained by a linear interpolation between the two values for the point of time measuring the attenuated flux S.

The magnitude of the unattenuated average count sample, $R_o(S_o)$, effectively determines the upper limit of optical depths beyond which no significant data can be expected. The precision to which optical depths may be determined is, of course, also related to the magnitude of R_o. In the interest of data quality, the system therefore does not produce optical depth data whenever the background-corrected signal becomes less than five counts per 0.5-sec sample. This means that the system will seek optical depths only up to a certain highest applicable standard optical depth reference value, that is,

$$\tau_{MAX} \leq \ln(S_o/5) . \tag{6}$$

Hence this maximum is different for different wavelengths. If S_o for any wavelength is so low that none of the standard optical depths will be sought, processing for that wavelength is halted. Similarly, processing is also terminated for wavelengths whose S_o-eligible region extends over the whole pass.

3.3   Optical Depth Computation

3.3.1   GENERAL DESCRIPTION

Optical depth data in the absorption analysis are given in terms of the times of occurrence of optical depths corresponding to 16 specific reference values. These reference values are given in Table 2. Orbital parameters may be computed for

13

each time, and so the optical depth, altitude, latitude, longitude, and so on, are all associated via this time. Scale heights and time variations may be inferred from differences in these data, but such computations will not be discussed here. The most important reason for the use of a standard optical depth list is the substantial reduction of data quantity. Using this method, the information from an entire pass is compressed into data on 16 points while losing very little information. This enables follow-on processing to proceed without requiring excessive amounts of computer time or storage. In fact, the ability of the EUVS absorption system to scan through large time periods of existing measurements is due to this data comparison.

The EUVS data reduction system starts with either the smallest or greatest of the standard optical depth values depending on whether the actual attenuation is increasing or decreasing. The attenuation trend is known because the data reduction system finds the time corresponding to the lowest probing height (h_Q) in the pass (that is, close to point of highest attenuation) and has either computed or has had as input the direction of processing. In order to seek the largest or smallest optical depth point, the system performs a two-parameter, non-linear exponential regression of the form

$$\tau = Ae^{B\Delta t}, \tag{7}$$

where A and B are the fitting coefficients, and Δt is the time difference in seconds from the starting point of the regression. The time inverval over which this regression is taken depends upon the amount of signal change. For periods of rapid change, the interval is contracted, so that important features are not lost; for periods of slower change, the interval is expanded to improve the statistical accuracy. The details of determining this interval are given in the next section. The τ values are computed from the observed signals by Eq. (2), where S is the background-corrected signal. When the data fit has been completed, the endpoints (in optical depth) are checked to see if the reference point is contained in the interval. If so, the relation of Eq. (2) is inverted, and Δt is computed for the standard optical depth point being sought. Addition of Δt to the starting time of the interval then produces the time corresponding to the occurrence of one of the standard values of optical depths. The next optical depth point in the list then becomes the one sought, and the current interval is checked to see if that point is within the present fitting range. If not, the fitting interval is shifted, another regression performed, and so on, until the next point is reached. The fitting intervals overlap for part of their ranges to insure a smooth transition between regressions and the degree of overlap depending on the time interval. The interval lengths (overlap times) are given as one of the three sets 24(8) sec, 16(8), 8(4) sec where the numbers in parentheses

14

expose the overlap of successive fit intervals. When optical depth points are not attained or are skipped, such as when the satellite is always too high (or low) for the h_Q to correspond to those points, the system notes the condition and proceeds. As part of the results for each standard point, the standard error is computed and preserved as a measure of data quality. The fitting coefficients are also kept. For double passes, two records are produced, one for the upleg and one for the downleg, and for each leg all 16 standard points may be computed.

3.3.2 RANGE SELECTION FOR OPTICAL DEPTH REGRESSION

When the satellite is over the sunward side of the earth (solar zenith angle $\leq 90°$), the minimum ray height, h_Q, is falling or rising only as fast as the satellite itself, and so the changes in signal are relatively slow. However, as the satellite goes into or out of eclipse, the minimum ray height may fall or rise very rapidly. Obviously the rate of change is most rapid when the sun is close to the plane of the satellite orbit. The situation is then similar to the data acquisition in a rocket experiment. To prevent statistical fluctuations from distorting the results in the first case, and to prevent the loss of information caused by the use of the exponential in the second case, different sizes of fitting interval are required. The exponential function was used, rather than a linear or polynomial, because it more closely represents the true physical function, and thus can cover a wider range. This function represents the data well over ranges where the change in signal corresponds to nearly a full height of penetration into the atmosphere. To meet this requirement the fitting interval is shortened as the level of attenuation increases, because the scale height is then also decreasing.

The speed at which the signal changes depends on three factors: the wavelength; the current level of attenuation; the range of solar zenith angles ("χ-region").

The wavelength dependence is caused by the different values of absorption cross sections listed in Table 3. For this analysis it is sufficient to divide the wavelengths into two groups, that is, more rapidly attenuating wavelengths indicated by SENSITIVITY = 2 in Table 1 and less rapidly attenuating wavelengths indicated by SENSITIVITY = 1 in Table 1. The corresponding distinction is part of the reference data set for that wavelength.

The type of attenuation region (low, medium, high) for the standard optical depths being sought is the second factor determining the length of the fitting range. At higher optical depths, the scale height for a given wavelength, $H(\tau_\lambda)$, is generally smaller than the value $H(\tau_\lambda)$ for lower optical depth (lower kinetic gas temperature for lower altitudes). Therefore, the list of standard optical depths is divided into three sections: Low attenuation region (6 values of τ_{REF}, optical depth $0.033 \leq \tau \leq 0.25$), medium attenuation region (5 values of τ_{REF}, optical depth $0.35 \leq \tau \leq 1.50$), and high attenuation region (5 values of τ_{REF}, optical depth $1.75 \leq \tau \leq 4.5$) as shown in Table 2.

15

Table 3. Absorption Cross Sections for 14 of the 20 Standard Wavelengths for Which Aeronomical Results Have Been Created So Far

		Cross Sections (Mb)			
LL	λ_{nom} (Å)	O	O_2	N_2	Remarks or note of main absorbers
1	175	3.5		5.1	O and N_2
2	465	10.2		21.8	Much poorer than for No. 14
3	584	13.0		23.0	O and N_2
4	765				Problems of radiation hardening
5	855	7.2	13.4	36.0	O and N_2
6	1609		4.7		O_2
7	1457		14.0		O_2
8	1700				O_2 vibr. distrib. study
9	1730				O_2 vibr. distrib. study
10	1835				O_2 band abs. (difficult)
11	256	7.1		9.6	O and N_2
12	304	9.0		11.6	O and N_2
13	610	13.1		23.1	O and N_2
14	465	10.2		21.8	O and N_2
15	585	13.0		23.0	Poorer than for No. 3
16	1026		1.5[*]		O_2 (see Note 1)
17	977				Problems of radiation hardening
18	1216		0.01[**]		O_2 (see Note 2)
19	1600		5.7		O_2 (most observations)
20	1775				O_2 vibr. distrib. study

[*]Note 1: Absorption of H Ly-β at higher altitudes is complicated by absorption due to atomic oxygen.

[**]Note 2: The use of the nominal, constant value of 0.01 Mb is justified as first approximation only.

The final factor taken into account is the solar zenith angle. As was previously mentioned, the rate of change of τ increases with the solar zenith angle χ. Again, the range of χ is split into three regions:

χ_1: $\quad \chi \leq \arccos(0.1)$

χ_2: $\quad \arccos(0.1) < \chi < 95°$

χ_3: $\quad \chi \geq 95°$

The type of range chosen for any regression depends upon the three factors mentioned earlier. Although the experimenter could modify the column "SENSITIVITY" of Table 1, in all routine data reductions the fitting intervals were fixed as given in Table 4. As the lowest optical depths in the low-attenuation region are reached, say $\tau < 0.1$, the 24-sec width of the widest range can become inadequate. For this reason, the two lowest standard optical depth points are often missing. However, if the count sample for the specific wavelength is high (reducing statistical scatter) good values may be obtained even for the lowest standard value of $\tau_{REF} = 0.033$. With the exception of the lowest τ_{REF} values, the method of range selection does keep the statistical variability and true functional shape within an appropriate range for the regressions. Additionally, the number of data points included within each fit is kept high enough to avoid spurious, physically non-meaningful solutions and yet low enough to facilitate rapid processing of the several hundred regressions which are performed for each pass.

To provide as much uniformity to the regression as possible, three standard fitting types have been selected. They are listed in Table 4 under various combinations of the three factors discussed above. The first designated 24(8) above, uses a range of three major frames (24 sec, up to 48 data points) with one major frame overlap (8 sec, 16 points) of the previous regression range; the second, denoted 16(8), uses two major frames (16 sec, 32 points) one of which overlaps the previous range; the third, designated 8(4), uses one major frame (8 sec, 16 points) and one-half of a major frame as overlap (4 sec, 8 points). The number of points mentioned above refer to the maximum possible that will occur only for perfect TM data and constant aperture selection. When the EUVS instrument used aperture alternation (AE-C orbits up to orbit 860) 16 wavelengths instead of 8 were sampled and the corresponding numbers of points per wavelength are then halved. Most often, the maximum is indeed attained, because the occurrence of bad telemetry over a time interval as short as 24 sec would have to be very severe to have a major effect on more than one wavelength. Fortunately, this has rarely happened.

3.3.3 REGRESSION ALGORITHM

The algorithm used to fit Eq. (7) was a standard non-linear least squares fit to the exponential. A linear fit to the logarithm of optical depth could not be used because the optical depth values could be negative. While a negative optical depth has no physical significance (the atmosphere does not add ultraviolet radiation), such points can occur because of normal statistical variability of signals in the low attenuation region. To reject these points would thus cut off statistical fluctuations in one direction while leaving them intact in the other, thus distorting the statistical treatment of the data.

17

Table 4. Fitting Intervals for Various Combination of the Three Factors

X-region	Low Attenuation Region (Optical depth $0.033 \leq \tau \leq 0.25$)	Medium Attenuation Region (Optical depth $0.35 \leq \tau \leq 1.50$)	High Attenuation Region (Optical depth $1.75 \leq \tau \leq 4.5$)
(1) More Rapidly Attenuating Wavelengths (SENSITIVITY = 2)			
X_1 ($X \leq$ arccos 0.1)	24(8)	24(8)	24(8)
X_2 (arccos $0.1 < X > 95°$)	16(8)	16(8)	16(8)
X_3 ($95° \leq X$)	16(8)	8(4)	8(4)
(2) Less Rapidly Attenuating Wavelengths (SENSITIVITY = 1)			
X_1 ($X \leq$ arccos 0.1)	24(8)	24(8)	24(8)
X_2 (arccos $0.1 < X < 95°$)	24(8)	24(8)	24(8)
X_3 ($95° \leq X$)	16(8)	8(4)	16(8)

Note: 24(8) means, for example, that data for 24 sec are used with 8-sec overlapping with the previous regression range.

18

Non-linear regressions require an initial approximation. Like many other functions, the one used, required the approximation to be reasonably close to the result. The data points are collected monotonically in time (and thus in attenuation), and the initial approximation is that exponential which would generate the final optical depth in the range from the initial ones. Thus, the approximation for A is the average of the first three optical depth values to represent the initial point, and the approximation for B is the value required to generate the last point, which is represented by the average of the final three values. Since

Average (final) = Average (initial) exp $[B \cdot (RANGE)]$,

$B = \ln [(Average (final)/Average (initial))] / Range$.

This approximation procedure is very good in all regions having attenuated data, and speeds the regression considerably. However, in areas that are in the very low attenuation region, it sometimes occurs that the approximation for A would be negative. Since this would not lead to a good solution, the approximation of $A = 0.01$, $B = 0.04$ is used whenever this occurs.

The iterative process of a non-linear regression requires a number of statistical controls to ensure the validity of the results. Data filtering for erroneous data will be treated in Section 3.3.4, while the control of the fitting algorithm and the quality checking of its results will be covered here. To ensure against a singular system of equations or an insufficient number of points, the determinants computed and the number of data points within each regression are checked against preset minimum values which are the same as those used for the reference signal (S_o) determination. The tolerance for ending the iterative process is an input parameter which for routine data production was set at 1×10^{-5}. The maximum number of iterations permitted was 20. If any of the above conditions were not satisfied, the fit was rejected. Upon completion of the regression, the resulting coefficients were compared with the initial approximation values. If either of the coefficients was less than the initial approximation by a factor of 0.01, or exceeded it by more than a factor of 100, the fitting results were rejected. This was done to prevent the occurrence of physically non-meaningful solutions. The factor of 100 was chosen, because in the low attenuation region, fairly large factors are reasonable. In addition to these tests, another feature of quality assurance of the system deserves mention here. If the reference signal is low, the higher optical depths would correspond to a very small number of counts, leading to imprecision. For this reason, the system does not produce data for the highest values of τ_{REF} for certain wavelengths for which the result would be based on an essentially insignificant number of count samples. The method of achieving this was covered in Section 3.2.4. Within the frame of quality checks and data filtering discussed next, regions of relatively poor

19

data quality can still be used to extract whatever useful information may be contained, without risking inadvertent acceptance of erroneous results as a consequence. For values of τ_{REF} for which data are produced, the latter include identification of the standard error computed, to provide quantitative information on data quality.

3.3.4 DATA FILTERING

Data filtering for transmission errors, stuck bits, and so on, is more complex for the optical depth computation than for the reference signal determination. As the count sample drops, the magnitude of the error that will damage the analysis also drops. This means that for high signals, a low-order bit error will not affect the results significantly, that is, the effect will be no more than that of the normal statistical fluctuation of the error-free data. However, as the signal drops due to attenuation, the same low-order bit error may correspond to an erroneous signal which could be several orders of magnitude greater than the actual signal. Therefore, as the signal drops, the risk of significant errors increases and it becomes necessary to have a dynamic set of limit filters. This is discussed next.

The absorption analysis data reduction system uses a pair of filters for each wavelength, one high limit and one low limit. Each limit is essentially a predicted signal, plus or minus several deviations, and is changed whenever the regression has accomplished data for one of the standard optical depth points. The signal prediction for these limit computations is subject to the same factors that determine the fitting interval, that is, the wavelength, the attenuation level, and the rate of change of the latter. The distinction of wavelengths has already been taken into account because each wavelength has its own set of upper and lower limit filters. Since the optical depth is a measure of the attenuation level, all that is required for the optical depth prediction is an estimate of rate of change of the optical depth. This estimate is based on the solar zenith angle. For not too large zenith angles, $\chi < \arccos 0.1$, the adopted system assumes that the signal may diminish to a value as low as that for three steps of τ_{REF} above the value of τ_{REF} just attained. That is, when one optical depth point has been filled, the next is then sought and the new low limit is adjusted to pass appropriately lowered signals. The corresponding optical depth displacement for the ranges $\arccos 0.1 < \chi < 95°$ and $\chi > 95°$, is four and five steps, respectively. The predictions need never be set to an optical depth higher than the maximum of $\tau_{REF} = 4.5$ listed (see Table 2). When that point is filled, no more data of that wavelength in the given pass will be processed. The actual filter progression is based on passing variations within a stated permitted range of deviations as discussed below.

Once the estimate of projected value, τ_{est}, is obtained, it is used to determine a signal by the equation

$$S_{est} = S_o e^{\tau_{est}}.$$

(8)

20

From this signal, the <u>lower limit</u> is obtained by subtracting a certain number of deviations. Each deviation is defined as the square root of the predicted low signal. The actual number of deviations is an input parameter but was set equal to 5 for all routine data production.

The estimate of an appropriate <u>upper limit</u> is obtained by using the τ_{REF}-point just attained (with no offset). The new upper limit is then obtained by adding the aforementioned number of deviations to the signal determined for the last τ_{REF} value. The process for updating limits when the optical depth is decreasing (sunrise) is analogous. However, now the upper limit has the offsets of three, four, or five steps in τ_{REF} and the lower limit is based on the τ_{REF}-point just attained. Again, it is not necessary to go beyond the boundaries of the τ_{REF} list (see Table 2). If at any time the predicted lower limit of a signal is less than 60 counts, that limit is set to zero. Immediately after the computation of the unattenuated reference signal, the limits are set as wide as possible (lower is zero, upper is S_o plus 5 deviations) because the first optical depth point to be attained is unknown until it is reached and the limit updating procedure above takes over. Each time a violation of one of the limits occurs, the point is rejected and the recorded count of violations is increased by one. Separate counts are maintained for upper and lower limit violations. There is also a counter for "fill" data, that is, where TM data of geophysical significance do not exist (having been replaced by a specific flag indicating that condition). All three of these counter values are carried into the data file record produced.

4. PRODUCTION OF ALTERNATIVE OPTICAL DEPTH DATA (LMC85)

4.1 Introduction

The EUVS absorption-data production program named LMC85 creates records of considerably greater detail than those produced by the standard program named LMC80 which creates data for up to sixteen standard values of optical depths only. The two programs differ in several important aspects. The program LMC85 creates time-ordered records of optical depths for input-controlled fixed steps in time, whereas LMC80 creates records for the times of occurrence of certain standard optical depths only. Typical values of the fixed-time increment chosen for LMC85 are 5 or 15 seconds, selected to facilitate the comparison with the so-called "United Abstract Data" (UA data) on results of other AE-satellite experiments given with a standard granularity of 15 seconds. Results of EUVS observations are not conducive to this type of presentation, mainly because of the need for a total number of words per timepoint in excess of the acceptable allotment for each experiment.

21

Therefore, it was decided that standard UA file records would not be written for the EUVS experiment.

Therefore, the records created by the program LMC85 represent a superior substitute for otherwise non-existent UA file data on EUVS absorption results. However, for economical reasons, no attempt can be made at any quasi-duplicate application of LMC85 approaching even remotely the complete coverage provided by the standard optical-depth-data production of LMC80. Fortunately, the latter represents quite adequate scientific information for most purposes. Hence, the execution of the program LMC85 is expected to remain restricted to special cases. The output of LMC85 represents "stand-alone files." This means that these file records, written in EBCDIC format, contain all of the important geophysical parameters of interest for each point in time for which the optical depth was evaluated, that is, the effort of scientific access to these results (stored on magnetic tape) does not require any read program with access to any additional data such as orbit-attitude or solar ephemeris data. The format of these files is specified in Section 4.3.

Unlike LMC80, the program LMC85 produces optical depth data for uniformly spaced time points of the entire period of observations made during a given pass. Both the unattenuated reference signal (S_o) and the optical depths are computed from time-based linear regressions. The optical depth data reduction can be specified to start at some specific data and time, with optical depths being extracted for uniform time intervals which are usually specified as 15 or 5 sec, depending on the desired resolution. Thus, the results of this portion of the analysis may be directly compared with other time-based regular data bases such as the Unified Abstract (UA) files from the Atmosphere Explorer project. The results of this analysis are especially useful in the very low attenuation region where the standard data production program LMC80 is not particularly useful. For these cases the data-fitting range of LMC85 may be expanded and the form of the linear regression for low attenuation usually matches the true change in the date more closely than does the exponential regression used by LMC80. In addition, LMC85 incorporates model-based corrections for data on S_o taken from a region where the signals are significantly attenuated, in order to provide a better value of optical depths calculated with the so corrected value of the unattenuated reference signal S_o. Another important application of the program LMC85 is its occasional use for diagnostic comparison of its results with those obtained by the standard program LMC80. This provides a valuable check on the results of both systems, as they both operate on the same observational data base.

22

4.2 Determination of "Unattenuated" Reference Signal (S_o)

4.2.1 RANGE SELECTION

As in the standard data reduction system (LMC80), the reference signal for each wavelength processed by the special program LMC85 may be determined in several ways; however, only one S_o-eligible region is used for each wavelength, and all of the wavelengths using a specific method also share a common S_o-eligible region. Each wavelength may have its reference signal computed by: (a) direct entry of the raw reference signal, (b) automatic selection of an S_o-eligible region, or (c) entry of the time (and time span) of an "S_o-eligible region" from which the reference signal S_o will be extracted. For the entry of an S_o-eligible region, the experimenter enters the date and time of the center of the chosen region as well as the size of the time interval for the corresponding data fit. The resulting processing time interval then includes the given interval before the given time and the interval after it. All wavelengths for which this method has been chosen use this same interval. Typical intervals over which S_o is computed are of the order of 15 sec, corresponding to a total S_o-eligible region of 30 seconds. The interval used is carried into the file along with an indication of the method of S_o-range selected. For the direct entry of a raw unattenuated signal, a date and time must be included for use in obtaining the orbit data for the absorption correction described in Section 4.2.3. Each wavelength with the direct entry of a raw unattenuated signal can have a different date and time. The final method of S_o-eligible region selection (automatic selection by the program) is accomplished by selecting the time of minimum solar zenith angle. Since this section of the system is used primarily for near equatorial circular orbit conditions, the region of least attenuation can be simply selected by this method. There is no attempt to ensure a maximum tolerance of attenuation, since all S_o values receive a correction for this (see Section 4.2.3) and the magnitude of this correction is carried into the resulting data files. The exact S_o-time for the fitted value is then taken as the nearest 15-sec point to the time of minimum solar zenith angle. The size of the time interval is determined the same way as for a direct entry. Again, the given time range (in seconds) is taken both before and after the center of the region. If the center point of the region is less than the given interval from either end of the pass, or if the EUVS instrument is scanning for a flux study at that time, the S_o-eligible region is repositioned accordingly, again to a whole 15-sec point. As is the case for the direct entry method, all wavelengths for which this method has been specified will share the same S_o-eligible region, but this region need not be the same as that of the wavelengths processed with the direct-entry method, nor any of those wavelengths where the raw signal and a reference date and time have been given by the experimenter.

23

4.2.2 REGRESSION ALGORITHM

The value of the raw unattenuated signal for each wavelength is determined by a standard linear least squares regression of the form

$$S = A + B \Delta t . \tag{9}$$

In this equation, S is the raw signal, Δt is the elapsed time in seconds from the start of the fitting interval, and A and B are the regression coefficients. The same checks for the minimum number of points and for the insignificant determinants are performed as in the standard data reduction system (LMC80). The unattenuated raw signal is taken from the center of the fitting interval, and the standard error is computed and kept in the same record with the data.

4.2.3 FINAL S_o DETERMINATION AND BACKGROUND CORRECTION

Once the raw unattenuated signal is extracted for each wavelength, it is corrected for background by the same algorithm as was used in the regular data production system (see Section 3.2.3). However, after this has been done, the resulting signal is corrected for residual attenuation by the atmosphere. This correction is obtained by the use of one of the models mentioned below to predict particle number densities of O, O_2, N_2, and He. From these, constituent-associated optical depths are computed and summed to find a predicted total value of optical depth for "S_o." Once this optical depth, τ_o, has been obtained, the corrected value of $(S_o)_{corr}$ is obtained from the relation

$$(S_o)_{corr} = S_o e^{\tau_o} . \tag{10}$$

Three different atmospheric models may be used to generate the predicted value of $\tau_o(S_o)$, that is, the MSIS model, see Hedin et al,[3,4] the Jacchia 1971 model, or a default model which uses an input temperature and set of densities at a given reference height along with an assumed exosphere temperature and "shape factor" to generate the final densities using a "Bates profile." The constituent optical depths and an indication of the model used to compute them are carried into the output, so

3. Hedin, A.E., Salah, J.E., Evans, J.V., Reber, C.A., Newton, G. Spencer, N.W., Kayser, D.C., Alcayde, C., Bauer, P., Cogger, L., and McClure, J.P. (1977) A global thermospheric model based on mass spectrometer and incoherent scatter data, MSIS 1, N_2 density and temperature, J. Geophys. Res. 82(No. 16):2139-2147.

4. Hedin, A.E., Reber, C.A., Newton, G.P., Spencer, N.W., Brinton, H.C., Mayr, H.G., and Potter, W.E. (1977) A global thermospheric model based on mass spectrometer and incoherent scatter data, MSIS 2, composition, J. Geophys. Res. 82(No. 16):2148-2156.

that the correction may be removed and another one substituted using a different model whenever this may become desirable at some later time. For most purposes, the MSIS model was used, and the default model was used only for testing purposes. Although the model used has errors in the predicted number densities that can be quite large, the effect upon the S_o data is usually small. For S_o regions which are nearly unattenuated, the predicted optical depths will be so small that the data will be unaffected even if the predicted optical depth were doubled. In regions where a significant absorption correction is required, there will be a more significant effect upon the data. If the true correction required was 15 percent and the model is 30 percent off, the resulting value of S_o would then still be only 5 percent away from the true value of S_o. As the correction required for atmospheric absorption increases, the net error due to model inaccuracy will of course increase. Therefore LMC85 was indeed not used for any passes where the raw S_o-signal required a massive correction.

In order to convert the model-predicted particle number densities for each constituent (j) into optical depth, the following relation was used

$$\tau_j = \sigma_j n_j H_j F_j .$$

(11)

In this equation, n_j is the predicted particle number density, σ_j is the absorption cross section for the wavelength being corrected for that constituent, H_j is the partial pressure scale height of that constituent, and F_j is the so called optical-depth factor required to convert the vertical optical depth, $\tau_{v,j}$ ($\tau_{v,j} = \sigma_j n_j H_j$) to the optical depth τ_j for the given slant column, ($\tau_j = \tau_{v,j} F_j$). The scale heights H_j are computed from the relation

$$H_j = \frac{kT}{m_j g} ,$$

(12)

where k is the Boltzmann constant, T is the kinetic gas temperature predicted by the model, m_j is the mass of the constituent j, and g is the gravitational acceleration adjusted for the altitude of the measurement. The function F_j varies depending upon the solar zenith angle χ, and the scale height.
For $\chi \leq 70°$

$$F_j = F = \sec \chi .$$

(13)

For $70° < \chi < 105°$

$$F_j = \sqrt{\frac{\pi}{2} \frac{R_e + h_Q}{H_j}} \left(1 + \frac{3}{8} \frac{H_j}{R_e}\right) e^{\frac{h_s - h_Q}{H_j}} \left[1 - \text{erf} \sqrt{\frac{h_s - h_Q}{H_j}}\right] .$$

(14)

25

For $\chi \leq 105°$

$$F_j = \sqrt{\frac{\pi}{2} \frac{R_e + h_Q}{H_j}} \ (1 + \frac{3}{8} \frac{H_j}{R_e}) \left[1 + \text{erf} \sqrt{\frac{h_s - h_Q}{H_j}} \right]. \tag{15}$$

These equations assume a spherical atmosphere, and compute a correction to the optical depth at the point of minimum ray height, h_Q. The point Q is called remote probing point for $\chi > 90°$, whereas Q is identical with the actual satellite point for $\chi \leq 90°$ (see Figure 1).

Upon the completion of the above correction process, (summing τ_j for all constituents), the S_o value, its date and time, its corresponding orbit data, and the experimenter input controls are written to the output file. All of the orbit data used in the computations and for output have been corrected for possible instrumental misalignment by a process described in detail in Section 4.5.

4.3 Optical Depth Computations

4.3.1 RANGE SELECTION

Optical depth data are computed, regressions performed, and the resulting fitted values at the requested time intervals are reported, along with associated orbit parameters. The format of each entry generated in the data file is specified in Table 5. There can be any number of these entries following the entry for S_o and its associated parameters. Two time intervals in sec are given by the user of the program LMC85. The first is the data-taking interval, T. The system takes data starting from the given starting date and time through the ending date and time once in each interval. These times are synchronized to 0 sec on the starting date, that is, the first point occurs for a time t = N.T, where N is the lowest integer value that will give data within the pass. The volume of data received depends solely upon this parameter. Intervals which are fractions or multiples of 15 sec are particularly useful, as they enable direct comparisons of EUVS data with the Atmosphere Explorer Unified Abstract data base. The actual parameter used for any given reduction is given in the last section of the S_o entry for that pass. This interval is the same for all wavelengths under analysis and has no effect upon the length of the fitting interval which may overlap the adjacent ones. The latter is determined by the second time interval given by the program user and it works in the same way as that for the S_o-computation. This means that all data from that interval before, to the interval after, are included in the regression. The latter interval selection is also reported in the S_o-associated entry. It is independent of the corresponding interval selected for the S_o-computation.

26

Table 5.   File Format for Optical Depth Special Studies Files

99999	-	Flag indicating next 4 records of the S_o format, and all subsequent optical depth records will refer to it.
S_o Record 1	-	S_o Results
F8.2		S_o (Counts)
F6.2		Background (Counts)
F5.3		Optical depth correction for constituent O
F5.3		Optical depth correction for constituent N_2
F5.3		Optical depth correction for constituent O_2
F5.3		Optical depth correction for constituent He
A1		Satellite ID (C, D, or E)
I5		Date of S_o (Julian day yyddd)
I8		Time of S_o (milliseconds)
A4		Method of S_o eligible region range selection
		CPT1 - automatic (lowest solar zenith angle)
		EN1R - entry of region
		DIPT - direct entry of raw value and time
S_o Record 2	-	S_o Regression Results
1PE10.3		Zero order regression coefficient (A)
1PE10.3		First order regression coefficient (B)
OPF6.2		Standard Error of regression
I3		Number of points in regression
I3		Number of upper limit violations
I3		Number of lower limit violations
S_o Record 3	-	Orbit Parameters
I5		Orbit Number
F6.2		Solar Zenith Angle (deg)
F7.2		Minimum Ray Height (km)
F7.2		Satellite Height (km)
F6.2		Remote Probing Point Latitude (deg)
F7.2		Remote Probing Point East Longitude (deg)
F6.2		Remote Probing Point Dipole Latitude (deg)
I6		Remote Probing Point Local Solar Time (hhmmss;hours minutes seconds)

Table 5. File Format for Optical Depth Special Studies Files   (Cont)

S_o Record 4 - $F_{10.7}$, Ap, and input parameters	
F5.1	$F_{10.7}$ Daily Average for S_o date
F5.1	$F_{10.7}$ Daily Average for Day prior to S_o date
I3	Average Ap value for 9 to 6 hr prior to S_o time
I3	Average AP value for 6 to 3 hr prior to S_o time
I3	Average Ap value for 3 to 0 hr prior to S_o time
I3	Average Ap value for 3 to 0 hr prior to S_o time
I6	Reference file key ID (yymmdd)
I6	Model and Cross Section Reference file key ID (yymmdd)
I6	Date of System Execution (yymmdd)
F4.1	Range (in sec) around S_o center data and time
F4.1	Range (in sec) around optical depth date and time
F4.1	Data taking interval for optical depths (sec)

Each Optical Depth Entry comprises two records of the following format, and are indefinite in number for each S_o entry.

Optical Depth Record 1 - Optical Depth and Regression Results	
I5	Date of Optical Depth Point (yyddd)
I8	Time of Optical Depth Point (msec)
F7.3	Optical Depth Value
1PE10.3	Zero order regression coefficient
1PE10.3	First order regression coefficient
OPF6.2	Standard error of regression
I3	Number of points in regression
I3	Number of upper limit violations
I3	Number of lower limit violations

Optical Depth Record 2 - Optical Depth Orbit Parameters	
F6.2	Solar Zenith Angle (deg)
F7.2	Minimum Ray Height (km)
F7.2	Satellite Height (km)
F6.2	Remote Probing Point Latitude (deg)
F7.2	Remote Probing Point East Longitude (deg)
F6.2	Remote Probing Point Dipole Latitude (deg)
I6	Remote Probing Point Local Solar Time (hhmmss:hours minutes seconds)

4.3.2 REGRESSION ALGORITHM

Optical depth data are obtained from standard linear least squares regressions of the form

$$\tau = A + B\ \Delta t \ . \tag{16}$$

In this equation, Δt is the time in elapsed seconds since the start of the fitting interval, and A and B are regression coefficients. As in the standard program (LMC80), the optical depths, τ, at each point are determined as

$$\tau = -\ \ell n\ (S_0/S) \ , \tag{17}$$

where S_0 is the corrected unattenuated signal discussed above. The same checks for a minimum number of data points or singular system are made as in the S_0 regression, and the standard error is also computed and reported in each optical depth entry made in the resulting data files.

4.4 Data Filtering

In keeping with the special nature of the program LMC85, the upper and lower limits for data acceptance are left somewhat wider than they are for the standard program LMC80. Only for the S_0 computations, the data filtering is performed in the same way as in LMC80, that is, reference values of upper and lower limits are used for each wavelength. Afterwards, in the optical depth computations, the lower limit is set to zero, and the upper limit is set to a value given as

$$S_{\text{upper limit}} = S_0 + 5\sqrt{S_0} \ . \tag{18}$$

This method is used to eliminate, not merely so-called fill data, but also data which are grossly aberrant, for example, due to transmission errors of "stuck-bit" problems.

As was the case in the standard data production (LMC80), the magnitude of the instrumental count sample for S_0 determines the practical maximum value of optical depths that can be evaluated. Again, data for optical depths corresponding to a signal of less than five counts (after background correction) will not be placed in the output files.

29

4.5 Alignment Corrections to Orbit Data

4.5.1 RATIONALE

The EUVS instrument is pointed by the Solar Pointing System (SPS) at any one of 256 different target points covering a square angular field slightly greater than the solar disk. For routine geophysical observations, the target is selected close to the center of the solar disk. Due to finite mechanical tolerances, there are some slight departures from exact co-alignment for each of the 24 monochromators of the EUVS instrument. As a result, each monochromator entrance axis has some slight angular departure (on the order of several minutes of arc) from the axis of SPS pointing, and thus, for narrow-field monochromators, a slightly different effective value of solar zenith angle. These small differences in the solar zenith angle lead to correspondingly small changes in the minimum ray height (h_Q) at which data are taken by each monochromator (see Figure 1). This effect is negligible for those monochromators with full disk view of the sun. Even for narrow-field monochromators, these departures are quite significant for large values of h_Q (where the scale height is large). However, for high solar zenith angles, the effective value of the remote-probing height h_Q from that of perfect coalignment may be several kilometers. This effect is obviously more serious for wavelengths penetrating deeply into the atmosphere, for example, H Ly-α, where the scale heights are low and the absorption increases rapidly once attenuation begins. This problem is handled by computing corrected solar zenith angles and minimum ray heights separately for each monochromator, that is, for each wavelength. All other orbit parameters included in the data file (latitudes, longitudes, local solar time, and so on) are also computed for these corrected values of solar zenith angle, although the small differences in the latter are usually not significant.

4.5.2 ALGORITHM

In order to compute the true solar zenith angle for those wavelengths which can have a significant deviation, a data set of offsets is provided (one each for the ϵ - and γ - directions respectively) for each. These offsets were determined from occasional diagnostic modes of operation called "raster scan," where the SPS target point rasters across the solar disk. An evaluation of the responses of the various monochromators during such a raster then allows one to determine the offsets of each monochromator-entrance axis with respect to the ideal point direction. The resulting offsets expressed in SPS steps were then converted to angular offsets in the ϵ - and γ - directions and placed in a table for use by the program LMC85 and other programs (see Table 6).

Detailed discussion on the correction for solar alignment of monochromators and the effects of fields-of-view are shown in Appendix A, Sections A1 and A2, respectively.

Table 6. Alignment Offsets for AE-C in Radians

	Wavelength	Epsilon	Gamma
1	175 Å		
2	465		
3	584	No correction required	
4	765		
5	855		
6	1609	-0.00206	+0.00124
7	1457	-0.00206	+0.00124
8	1700	-0.00206	+0.00124
9	1730	-0.00206	+0.00124
10	1835	-0.00206	+0.00124
11	256	-0.00204	+0.00162
12	304	-0.00204	+0.00019
13	610	-0.00204	+0.00117
14	465	-0.00204	+0.00099
15	584	-0.00219	+0.00158
16	1026	-0.00198	-0.00147
17	977	-0.00204	-0.00195
18	1216	-0.00097	-0.00007
19	1600	-0.00369	+0.00022
20	1775	-0.00369	+0.00047

NOTE: For AE-C orbits after 860, the EUVS instrument
was offset 7 arc min in the positive epsilon
direction to improve the pointing of the narrow
field-of-view monochromators, that is to have
them point more closely to the center of the
solar disk. Therefore, this offset (0.0020362175
radians) was added to the epsilon offset for
these orbits.

5. MODEL COMPARISON (PROGRAMS LMCURSI and LMCIAGA)

5.1 Introduction

The purpose of the model-comparison programs (LMCURSI which accesses
LMC80 produced data and LMCIAGA which accesses LMC85 produced data) is to
provide a comparison of several atmospheric models with the EUVS-derived results
on optical depths for varying conditions. To accomplish this, the model-predicted
particle number densities for atomic oxygen, molecular nitrogen, molecular oxygen,

31

and helium are converted to both a total optical depth and a three-constituent optical depth (adding contributions by O, N_2, and O_2 only) using a standard data set of absorption cross sections. The ratios of these model-values of optical depths to the values derived from the EUVS observations are then determined. These ratios, along with all other associated details including identification of model and list of all relevant geophysical parameters for each point in time, are then sent to output files in the EBCDIC format. In addition to the ratios, each entry contains the date and time, the constituent optical depths generated from the selected model, the total optical depth from EUVS, the helium contributed optical depth used with it, and the associated orbit parameters. An example of the actual output of the program LMCURSI is given in Table 7.

Any one of three models may be selected by the experimenter, and the resulting file entry indicates which model was selected. These are: the MSIS model[3]; the 1971 Jacchia model (CIRA 1972); or a so called "default"-model which is a simple test model in which the user of the programs selects a reference altitude, the constituent particle number densities, and temperature at that reference altitude as well as a shape factor (using a "Bates" profile) and an exosphere temperature. These input parameters are then used by the default model to generate the constituent densities and scale heights at any other altitudes for which model-based values of optical depths are desired. It should be noted that this default model provides no adjustments for diurnal, latitudinal, seasonal, or other types of atmospheric variabilities. This means that this default model is strictly an ad hoc utility allowing experimentation with various sets of model inputs such as may be desired for a detailed study of one specific set of observations.

5.2 Optical Depth Generation and Model Considerations

Although the programs LMCURSI and LMCIAGA produce a similar result, they operate on different data bases.

LMCURSI uses so-called "GU files," that is, the binary files generated by the standard program LMC80. Due to the compact form required for these GU file records, they have none of the associated orbit parameters and they do not provide regular coverage in time. However, due to the compactness of these GU files and the regular coverage provided, a wide range of geophysical conditions can be explored in a single execution of LMCURSI.

Table 7. Example of Output of Model - Comparison Program (LMCURSI)

NAME = UEY15 ("E" vehicle, standard wavelength No. 15, λ = 585 Å)														
DATE	TIME	TAU-OBS	TAU-HE	% ERR	TAU-NCR	MODEL	TAU-TOT	RATIO	TAU-3	RATIO	TAU(O1)	TAU(N2)	TAU(O2)	TAU(HE)
SZA	HQ	HS	QLAT	QLONG	QMLT	QLOC								
76300	79102192	0.574	0.041	8.74	0.548	MSIS	0.762	1.240	0.702	1.224	0.418	0.284	0.000	0.060
50.30	194.29	199.29	-10.80	-102.20	-1.10	152538								
76300	79353056	1.722	0.041	5.63	1.847	MSIS	2.237	1.289	2.177	1.264	1.106	1.071	0.000	0.060
86.05	177.48	177.48	-15.35	-85.55	-4.33	163635								
76303	71166240	0.160	0.042	19.76	0.150	MSIS	0.404	2.003	0.344	2.151	0.326	0.018	0.000	0.060
95.32	324.62	353.89	18.39	154.03	9.99	61828								

NOTE: Abbreviated letters appeared above are:

DATE = yyddd
TIME = in millisecond
TAU-OBS = observed τ (S_o is corrected from the model)
TAU-HE = τ for He model value at the place of S_o
% ERR = standard deviation for TOU-OBS calculated from the LE580 output
TAU-NCR = standard τ (non-corrected, that is, $S_o = 0$) see Table 2
MODEL = name of model used; MSIS, JA71, and so on
SZA = solar zenith angle
HQ = height of the remote probing point (h_Q)
HS = height of the satellite (h_s)
QLAT = latitude of the remote probing point Q

QLONG = longitude of the remote probing point Q
QLOC = solar local time at the remote probing point Q (in HH:MM:SS)
TAU-TOT = τ_{total}, calculated from the model and our cross section data
RATIO = ratio between TAU-TOT and (TAU-OBS + TAU-HE)
TAU 3 = τ_3, total of three constituents O, N_2 and O_2
RATIO = ratio between TAU-3 and TAU-OBS
TAU(O1) = τ_o; τ for O model value at the place of τ_{obs}
TAU(N2) = τ_{N_2}; τ for N_2 model value at the place of τ_{obs}
TAU(O2) = τ_{O_2}; τ for O_2 model value at the place of τ_{obs}
TAU(HE) = τ_{He}; τ for He model value at the place of τ_{obs}

33

Since many of the S_O-eligible regions were directly input, that is, selected in spite of significant residual optical depth to increase the rate of data return, a correction for these residual optical depths, $\tau_O(S_O)$, is performed at this level. The optical depth of each S_O date and time is computed from the model-predicted densities and temperatures by using the same algorithm described in Section 4.2.3 and is used as the $\tau_O(S_O)$. That is, the value of $\tau_O(S_O)$ is added to the standard optical depth values of each GU file entry within that pass. Thus the program LMCURSI generates values of corrected optical depths corresponding to more truly unattenuated S_O values. For double passes, where two S_O values are available, both residual optical depths are computed, and the final τ_R used for each optical depth point is the linearly interpolated value between them. For the sake of consistency, the same model is used for the τ_R computation as that requested for the ratio comparison.

Since the LMC85-created special study files already contain a residual optical depth correction, the model-comparison program LMCIAGA operating on these files first removes the LMC85-inserted model correction, and in its place, a new correction is performed with that model which is specified for the present execution of LMCIAGA.

34

References

1. Hinteregger, H.E., Bedo, D.E., and Manson, J.E. (1973) The EUV spectro-photometer on Atmosphere Explorer, Radio Science 8(No. 4):349-359.

2. Hinteregger, H.E., and Chaikin, L.M. (1977) EUV absorption analysis of thermospheric structure from AE-Satellite observations of 1974-1976, COSPAR Space Research 17:525-532.

3. Hedin, A.E., Salah, J.E., Evans, J.V., Reber, C.A., Newton, G.P., Spencer, N.W., Kayser, D.C., Alcayde, C., Bauer, P., Cogger, L., and McClure, J.P. (1977) A global thermospheric model based on mass spectrom-eter and incoherent scatter data, MSIS 1, N_2 density and temperature, J. Geophys. Res. 82(No. 16):2139-2147.

4. Hedin, A.E., Reber, C.A., Newton, G.P., Spencer, N.W., Brinton, H.C., Mayr, H.G., and Potter, W.E. (1977) A global thermospheric model based on mass spectrometer and incoherent scatter data, MSIS 2, composition, J. Geophys. Res. 82(No. 16):2148-2156.

5. Garriott, O.K., Norton, R.B., and Timothy, J.G. (1977) Molecular oxygen concentration and absorption cross sections in the thermosphere derived from extreme ultraviolet occultation profiles, J. Geophys. Res. 82(No. 32):4973-4982.

Appendix A

**Correction for Solar Alignment of Monochromators
and Effects of Fields-of-View**

A1. CORRECTIONS FOR SOLAR ALIGNMENT OF MONOCHROMATORS

The solar pointing subsystem (SPS) establishes a reference-target point on the solar disk with an accuracy of about 0.0003 radian. Figure A1 gives a schematic overview of geometrical relationships. The actual dimensions of the fields-of-view of the so-called "narrow-field monochromators" are still relatively large, for example, 0.001 radian for the monochromators No. 12, No. 23, and No. 24 in both elevation (ϵ) and cross-elevation (γ) and range up to 0.003 radian for some other narrow-field MN's of the EUVS instrument. Detailed illustrations of all relevant geometrical aspects are given in Figures A2, A3, and A4. Therefore the absolute SPS-associated pointing accuracy is indeed quite adequate. However, some of the narrow-field MN's on the AE-C satellite were found to have individual entrance axes departing from the SPS-pointing direction by angles ranging up to 0.0036 radian in ϵ direction and about 0.002 radian in the γ direction (see Figures A1 and A2) for the worst cases. The actual values of the MN-peculiar misalignment angles have been determined by evaluation of data obtained in diagnostic modes of operation of the SPS, that is, from 16-step ϵ-scans, 16-step γ-scans and 256-step full raster scans. The accuracy of this determination is estimated to be equal to that of the SPS accuracy, that is, also about 0.0003 radian. Within that accuracy, no changes of these misalignment angles were expected (considering the design) and none were indeed observed. The accuracies quoted had to be accepted as adequate for the objectives of aeronomical EUV absorption analysis planned for the EUVS experiment,

37

even though they would of course be considered unacceptably poor for instruments with truly narrow fields-of-view.

Whereas the selection of fields-of-view of less than about 1 arc min would have been clearly undesirable for aeronomical EUV absorption analysis (see Garriott et al)[5], fields significantly narrower than those of the EUVS instrument for AE would of course have been desirable, along with a better accuracy of monochromator co-alignment and somewhat better absolute accuracy of verifying SPS-pointing directions. However, the actual EUVS-design choices had to be made within rather strict constraints of cost, size, weight, power consumption, and lead-time to completion of instruments for flight, aside from the emphasis on full-disk measurements. These constraints necessitated certain otherwise undesirable compromises the consequences of which are analyzed in Sections A1 and A2. The latter deals with the problems due to the relatively large fields-of-view per se, that is, problems which would remain even if co-alignment and SPS pointing had been absolutely perfect.

The situation of monochromator co-alignment in the EUVS instruments on AE-D (the spacecraft failed in January 1976) and AE-E (still operating) was significantly better than that for AE-C (operated until December 1978). Only for the AE-C EUVS, the departures of MN-peculiar pointing directions from the SPS-established reference direction exceed the possible error of experimental verification significantly. The AE-C monochromators also showed a significantly asymmetric pattern of target points around the SPS-established reference target. Therefore, geophysical routine observations from AE-C, originally planned to be made with center-pointing of the SPS (NE = NG = 8 in Figure A1), were changed to use a standard offset of two elevation steps, that is, NE = 10, NG = 8 in Figure A1, resulting in values of $\epsilon_{SPS} = 0.002036$ radian and $\gamma_{SPS} = 0$. For this mode of operation, retained for all geophysical observations after AE-C orbit 860 (March 1974), the pattern of MN-peculiar target points characteristic of the AE-C instrument represents optimum symmetry around the center of the solar disk and also shows significantly reduced extreme-values of MN-pointing departures from the solar vector, that is, none in excess of about 0.0015 radian. For both AE-D and AE-E, the corresponding optimum was indeed that of no offset from sun-center pointing of the SPS, with individual MN-misalignment angles eventually no greater than the estimated accuracy of their verification. Therefore, Section A1 is important for AE-D and AE-E data only because of its use in the evaluation of effects of the finite fields-of-view—discussed in Section A2.

Our correction of effective solar zenith angles and remote-probing heights, accounting for the known departures of the individual monochromator-entrance axes

5. Garriott, O.K., Norton, R.B., and Timothy, J.G. (1977) Molecular oxygen concentration and absorption cross sections in the thermosphere derived from extreme ultraviolet occultation profiles, J. Geophys. Res. 82(No. 32):4973-4982.

from the direction of the solar vector ($\vec{s}_1$ is defined to point from the satellite position to the center of the solar disk) are based on the relations

$$\vec{\gamma}_1 = (\vec{s}_1 \times \vec{a}_1) / |\vec{s}_1 \times \vec{a}_1|$$

$$\vec{\epsilon}_1 = [\vec{a}_1 - \vec{s}_1 (\vec{s}_1 \cdot \vec{a}_1)] / |\vec{s}_1 \times \vec{a}_1| \qquad\qquad (A1)$$

where the geometry of these unit vectors $\vec{\epsilon}_1$, $\vec{\gamma}_1$, $\vec{s}_1$, and $\vec{a}_1$, is illustrated schematically in Figure A1, with all relevant details shown in Figures A2, A3, and A4. The spacecraft-spin axis $\vec{a}_1$, pointing outward from the EUVS-mounting surface, also represents the outward-pointing direction of the "azimuth axis" of the biaxial SPS. The spacecraft spin axis was constrained to be perpendicular to the satellite-orbit plane, not exactly, but at least to an accuracy of about 1-2° for those periods for which EUVS observations have been validated as geophysical, that is, excluding data taken during certain operations for purposes of instrumental diagnostics, during periods of "spacecraft-turnaround" (explained below) or during imperfect pointing. More specifically, this restriction in geophysical validation excludes any observations made during times when the SPS was either too close to the physical stop of elevation motion (around G = 5°, referring to Figure A1(b) or too close to G ≐ 90°, where the view of the solar disk may be partially or fully obstructed. Since the true orientation of the spin axis in the standard inertial frame of reference was often known only to an accuracy no better than that of the aforementioned constraint to be perpendicular to the orbit plane (± 1-2°), the validation of observations as geophysical is restricted to the safe range of 7° < G < 87° even for orbits for which attitude data on $\vec{a}_1$ were reliable to better than 0.5°. The exclusion of values of G ≤ 7° of course also removes the occurrence of undeterminate expressions for $\vec{\epsilon}_1$ and $\vec{\gamma}_1$ in the relations (Figure A1) above.

The actual amount of data rejected by the exclusion of those for G ≥ 87° has been very small indeed. The maneuver of "spacecraft turn-around" (changing orientation of spin axis by 180°), required to prevent the otherwise inevitable increase of the angle G beyond 90° due to the precession of the satellite orbit, was ordinarily initiated at a time for which the nominal value of the SPS-gimbal angle G was not yet too close to 90°, say around 88°. During several orbits before and after the scheduled time of spacecraft turn-around, the EUVS experiment was therefore ordinarily switched off. As a result, the existing small amount of data for orbits with G > 87° reflects largely inadvertent observations due to errors in scheduling (for example, errors in orbit predictions for a week in advance).

Use of the simplifying approximation of assuming the spin axis to be truly perpendicular to the orbit plane (identified the unit vector of its normal, $\vec{n}_1$),

39

$$\vec{a}_1 \doteq \vec{n}_1 (\vec{n}_1 \cdot \vec{s}_1) / |\vec{n}_1 \cdot \vec{s}_1| = \vec{n}_1 \text{ sign } (\vec{n}_1 \cdot \vec{s}_1) \qquad (A2)$$

may appear crude, but the actual consequences for our purposes of calculating $\vec{\epsilon}_1$ and $\vec{\gamma}_1$ from the relations [Eq. (1)] are readily acceptable. The angles formed by the directions of $\vec{\epsilon}_1$ and $\vec{\gamma}_1$ with some fixed reference direction in the plane perpendicular to the solar vector, for example, the direction of the projected solar axis of rotation, do not need to be known very accurately—say to a few degrees. For instance, a rotation of $\vec{\epsilon}_1$ and $\vec{\gamma}_1$ by a full 5° in this plane which is the plane of drawing in Figure A1(a), would change the offset coordinates of a nominal target point only by about 0.0001 or 0.0002 radian if that target point is offset from null by 0.001 or 0.002 radian respectively, corresponding to 1 or 2 steps of SPS-offset. Since none of the MN-misalignment angles relative to the solar vector were greater than 0.003 radian even for the worst case of the AE-C MN's, the adoption of relation [Eq. (A2)] is indeed justified as long as one excludes the region of angles G < 7°, for which the instrumental accuracy of offset pointing by the SPS also begins to become marginal.

Defining the angle E as the elevation of the sun measured from the satellite's orbit plane and defining the sign of E as positive (negative) when the sun is on the positive (negative) side of the orbit plane, one finds $\sin E \equiv \vec{n}_1 \cdot \vec{s}_1$ and can write the relations [Eq. (A1)] with adoption of the approximation [Eq. (A2)] as

$$\vec{\gamma}_1 = \pm \vec{s}_1 \times \vec{n}_1 / \cos E \, ,$$

$$\vec{\epsilon}_1 = \pm \vec{n}_1 / \cos E \mp \vec{s}_1 |\tan E| \, . \qquad (A3)$$

where the upper or lower signs must be used for E > 0 or E > 0, respectively.

Defining the instrumental target point on the solar disk as the center of the area of the solar disk viewed by a given monochromator, one finds the unit vector of the direction from the satellite to that target point (briefly called "target vector" below) to be given as

$$\vec{t}_1 = (\vec{s}_1 + \epsilon \vec{\epsilon}_1 + \gamma \vec{\gamma}_1) (1 + \epsilon^2 + \gamma^2)^{-1/2} \, , \qquad (A4)$$

where $\epsilon = \epsilon' + \epsilon_{SPS}$ and $\gamma = \gamma' + \gamma_{SPS}$ are the offset coordinates of the instrumental point of a given monochromator relative to the center of the solar disk; ϵ' and γ' are the corresponding offsets relative to the SPS-established reference target; ϵ_{SPS} and γ_{SPS} are the coordinates of the SPS target relative to the center of the solar disk.

This expression of the target vector [Eq. (A4)] in connection with the relations [Eq. (A3)] defining the chosen offset-coordinate axes, has been used in all of our computer programs where solar zenith angles (χ) and remote-probing heights (h_Q)

40

are required to be referred to that particular solar ray which connects the center of the instrumentally viewed area of the solar disk with the point of observation (satellite). It should be noted that the same relations, [Eq. (A3)] and [Eq. (A4)], also serve as the basis for the assessment of the effects of finite fields of view discussed in Section A2.

The zenith angle associated with a given target point is then determined by the relation

$$\cos \chi = \vec{P}_1 \cdot \vec{t}_1 \tag{A5}$$

where $\vec{P}_1 = \vec{P}/P$ (with $P = |\vec{P}|$) is the unit vector of the direction from the earth's center to the satellite and $\vec{t}_1$ is the target vector (also unit vector) introduced above.

The "remote-probing point" associated with that target point on the solar disk is then determined by the geocentric position vector given as

$$\vec{Q} = \vec{P} - \vec{t}_1 P \cos \chi; \ \vec{Q} \ (\chi \leq 90°) \equiv \vec{P} , \tag{A6}$$

and the geocentric distance of the probing point is given by its absolute magnitude,

$$Q \equiv |\vec{Q}| = P \sin \chi; \ Q(\chi \leq 90°) \equiv P . \tag{A7}$$

The "probing height" is obtained as

$$h_Q = Q - R_E(\phi_Q); \ h_Q \ (\chi \leq 90°) \equiv h_{SAT} , \tag{A8}$$

where the standard reference ellipsoid is used to approximate the sea-level surface required for the calculation of the geocentric distance of the sub point, $R_E(\phi_Q)$. The latitude of the probing point is given as $\phi_Q = \arcsin (Q_Z/Q)$, where Q_Z is the north-polar component of $\vec{Q}$ in the standard inertial reference frame.

To illustrate the pecularities of different effects of elevation offsets (ϵ) and cross-elevation offsets (γ), one can set the normalization term $(1 + \epsilon^2 + \gamma^2)^{-1/2}$ appearing in Eq. (A4) equal to unity, without introducing any significant error in the calculation of the offset correction.

Using the relation $\cos \chi_0 = \cos E \cos \beta$, $\cos \chi = \cos (E + \epsilon) \cos(\beta + \gamma)$ from Figure A2, this correction may be obtained as

$$\Delta \cos \chi \equiv \cos \chi - \cos \chi_0 = \mp \epsilon \ \cos \chi_0 \ |\tan E| \mp \gamma \cos E \ |\sin \beta| . \tag{A9}$$

where the upper (lower) signs refer to E > 0 (E < 0); χ_0 is the uncorrected value of χ for $\epsilon = \gamma = 0$, and the expression

41

$$\sin \beta = \vec{P}_1 \cdot \{\vec{s}_1 \times \vec{n}_1\} / \cos E = \mp [1 - (\cos \chi / \cos E)^2]^{1/2} \tag{A10}$$

with the same assignment of signs (upper for $E > 0$), defines the quantity β as the angle between the geocentric satellite-position vector and the projection of the solar vector onto the plane of the satellite orbit (see Figure A2).

The relations [Eq. (A9)] and [Eq. (A10)] show that for each orbit there are four characteristic positions distinguished by vanishing or extreme values of the offset-related corrections as follows.

For one pair of opposite positions defined by $\sin \beta_1 = \sin \beta_2 = 0$, only the ϵ-offsets have an effect on χ. For these two positions the zenith angle goes through its extremes, that is, $\chi_{o,1} = \chi_{o,\min} = |E|$ (generally not important since $h_Q = h_{SAT}$) and $\chi_{o,2} = \chi_{o,\max} = 180° - |E|$ (satellite either in the dark or at position for lowest positive value of h_Q near sunset or sunrise depending on specific values of h_{SAT} and E). For these positions, the correction equals $\Delta \cos \chi = -\epsilon \cos \chi_o \tan E$ (see Figure A3).

The other pair of characteristic positions is defined by the condition $\sin \beta_{3,4} = \pm 1$. For these positions, only the γ-offsets have an effect. It is given as $\Delta \cos \chi = \pm \gamma$ (since $\chi_{o,3} = \chi_{o,4} = 90°$) (see Figure A4).

From the foregoing relations for the angle β and the offset coordinate axes $\vec{\epsilon}_1$ and $\vec{\gamma}_1$, one finds that the expression

$$\cos \Theta \equiv \pm |\tan E| \tan (\chi_o - 90°) \tag{A11}$$

defines the quantity Θ as the angle between the "vertical entrance plane" of the instrument (containing the vectors $\vec{t}_1$ and $\vec{Q}$) and the "meridional entrance plane" (containing the vectors $\vec{t}_1$ and $\vec{\epsilon}_1$). This meridional entrance plane also represents the "plane of dispersion" of the gratings in all EUVS monochromators. The entrance plane formed by $\vec{t}_1$ and $\vec{\gamma}_1$ is called "sagittel entrance plane" (parallel to the ruled lines of the planar diffraction gratings).

The Eqs. (A9) and (A11), combined with the relation $\Delta \cos \chi = - \sin \chi_o \Delta \chi$, can be used to express the "vertical angular shift" due to offsets of $\epsilon \neq 0$ and $\beta \neq 0$ in a more comprehensive form, that is,

$$\Delta \chi = - \epsilon \cos \Theta - \gamma \sin \Theta. \tag{A12}$$

where $\cos \Theta$ was given by Eq. (A11) and $\sin \Theta$ is, correspondingly, given as

$$\sin \Theta = \pm [1 - (\cos \chi_o / \cos E)^2]^{1/2} / \sin \chi_o. \tag{A13}$$

42

The corresponding effect in the remote-probing height is then given as

$$\Delta h_Q = (\epsilon \cos \Theta + \gamma \sin \Theta)\, P \sin U \,, \tag{A14}$$

where $U \equiv \chi_o - 90°$ is the nominal solar depression angle, the quantity $d = P \sin U$ represents the distance of the remote-probing point from the satellite instrument, and Θ is the angle between the vector $\vec{Q}$ and the ϵ-offset coordinate axis. Since this angle is not required to any accuracy better than a few degrees, the simplified calculation of its value (for $\chi = \chi_o$ and $\vec{a}_1 = \pm \vec{n}_1$) implied by the expressions for $\cos \Theta$ [Eq. (A11)] and $\sin \Theta$ [Eq. (A13)] above, is perfectly adequate. Our equation for Δh_Q [Eq. (A14)] is equivalent to Eq. (6) of the description of the EUVS experiment published before launch [Hinteregger et al (1973) noting that the Eq. (5) in the same report should show $\cos \theta$ instead of $\tan \theta$ written erroneously].

This section is concluded by giving an illustrative example in which the required corrections for offset pointing approach a magnitude characteristic of "worst cases," that is, AE-C observations made from high satellite altitudes and with solar depression angles close to 30°. Taking $\chi_o = 118°$, $P = 8500$ km, and $E = 60°$ with $\epsilon_{23} = -0.00105$, $\gamma_{23} = 0.00022$ for MN No. 23 and $\epsilon_{12} = -0.00002$, $\gamma_{12} = 0.00124$ for MN No. 12, respectively, one finds, with $\Theta \doteq 22.935°$, and $d = 3990$ km) Δh_Q (MN No. 23) $\doteq -5.72$ km and Δh_Q (MN No. 12) $\doteq +1.85$ km corresponding to a difference of almost 8 km for the corrected probing heights for simultaneous observations by MN No. 23 and MN No. 12.

In Figure A1, the plane of drawing (a) is perpendicular to the direction toward the center of the solar disk. The offset-pointing subsystem allows selection of any one of 256 target points. The elevation and cross elevation offset angles relative to central solar pointing are given as $\epsilon_{SPS} = (NE-8)\Delta\epsilon$ and $\gamma_{SPS} = (NG-8)\Delta\gamma$, respectively ($\Delta\epsilon = \Delta\gamma = 0.001018$ rad/step). The positive directions of the ϵ and γ axes are uniquely determined from the known directions of the spacecraft spin axis (unit vector of $+Z_{SC}$ axis equal to outward pointing unit vector of SPS azimuth axis designated $\vec{a}_1$) and unit vector of direction to center of solar disk ($\vec{s}_1$), for example, $\vec{\gamma}_1 = \vec{s}_1 \times \vec{a}_1 / \sin G$, as shown in the schematic (b). Since the spin axis $\vec{a}_1$ was routinely held within ± 1-$2°$ of the normal direction to the orbit plane, one finds $G \doteq 90° - |E|$ with $E > 0$ ($E < 0$) expressing the solar elevation over the satellite's orbit plane ($E < 0$ when sun is on the negative side of that plane), that is, setting $\vec{a}_1 = \vec{n}_1$ sign $(\vec{n}_1 \cdot \vec{s}_1)$, where $\vec{n}_1$ is the normal vector of the orbit plane.
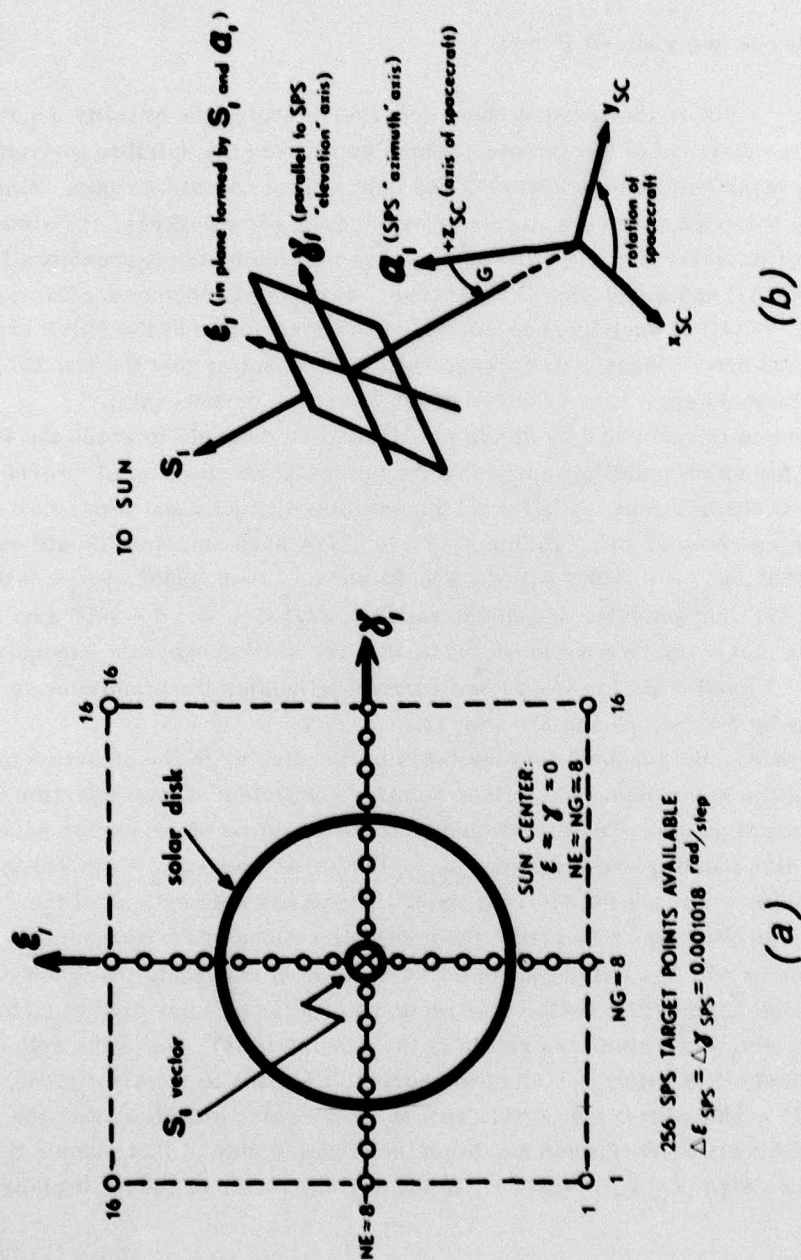
43

Figure A1. Solar Pointing Geometry

Various quantities used in the text are illustrated in Figure A2. SC = space-craft, O = center of earth, Q = remote probing point, R = radius of earth, h_Q = height of remote probing point, χ = solar zenith angle of the target point, χ_o = solar zenith angle of the center of the solar disk.

Figure A3 shows the spacecraft (SC) at the position where $\beta = 0°$, $\chi_o = 180-E$. Thus the γ-offsets have no effect on χ.

Figure A4 shows the spacecraft (SC) at the position where $\beta = 90°$, $\chi_o = 90°$. Thus the ϵ-offsets have no effect on χ.
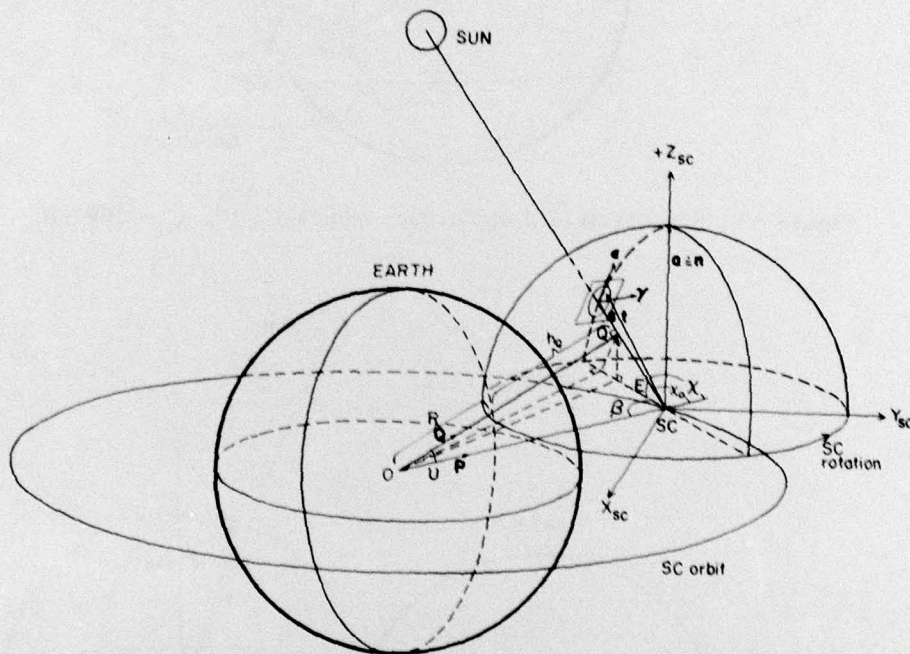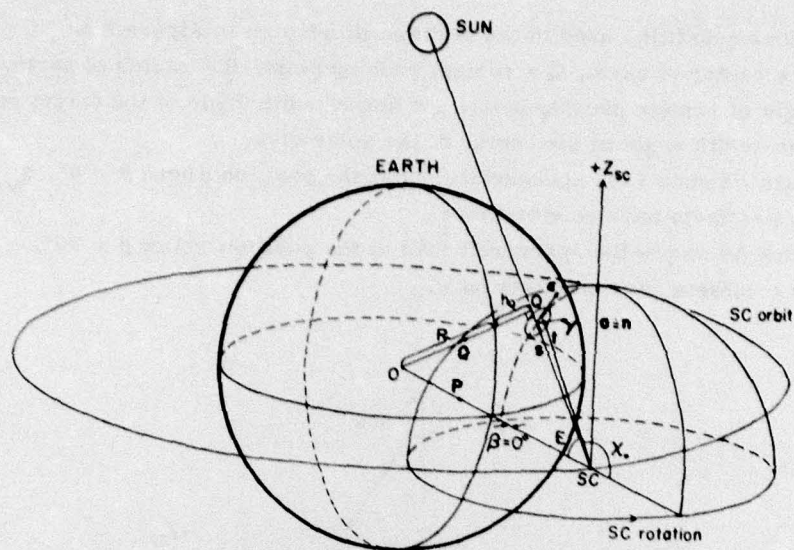

Figure A2. Various Quantities Used in Text

45

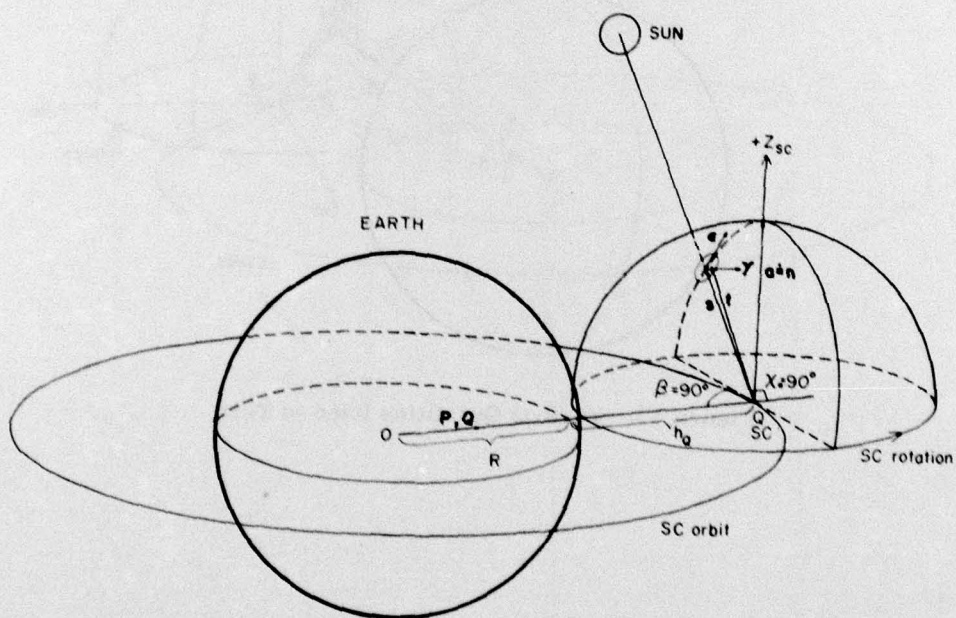Figure A3. Spacecraft (SC) at Position Where $\beta = 0°$, $\chi_O = 180° - E$

Figure A4. Spacecraft (SC) at Position Where $\beta = 90°$, $\chi_O = 90°$

46

A2. EFFECTS OF FIELDS-OF-VIEW

The effects of the field-of-view (FOV) for the so-called "full-disk mono-
chromators" and "reduced-field monochromators" are discussed separately below.
The monochromators of the first group had been designed with emphasis on the
measurement of incident EUV fluxes at all wavelengths, that is, using a wavelength-
scanning mode of 128-steps for each of the scan-capable monochromators. How-
ever, these scan observations have been scheduled only for those parts of an orbit
for which the combination of solar zenith angle and satellite height has been favor-
able in the sense of expecting only reasonably small corrections for atmospheric
attenuation. For the remaining time of instrument operation, all monochromators
have been kept in fixed wavelength settings, corresponding to certain standard steps
(step 64 for all EUVS-1 MN's, steps 64, 24, 88, 96, or 124 for all EUVS-2 MN's)
to provide the data desired for EUV absorption analysis of atmospheric structure.
Conversely, the reduced-field monochromators had been designed with primary
emphasis on EUV absorption analysis, and their use for observing temporal varia-
tions of incident solar EUV at these fixed wavelengths reflects only a secondary
objective in terms of aeronomical interest. The latter interest would of course
have preferred full-disk flux data rather than observations restricted to some small
central part of the area of EUV sources on the solar disk.

A2.1 Full-Disk Monochromators

Approximately one-half of the monochromators used in the EUVS instrument on
the Atmosphere Explorer satellites AE-C, D, and E are called "full-disk MN's,"
since their unencumbered field-of-view extends beyond the solar disk in both the
ϵ-direction (unencumbered meridional acceptance width of $\Delta\epsilon_U \doteq 0.0174$ rad) and
the γ-direction (sagittal width of $\Delta\gamma_U \doteq 0.0174$ rad). As can be seen in Figure A1,
these unencumbered widths are greater than the angle subtended by the photospheric
disk ($\Delta\epsilon_{SUN} = \Delta\gamma_{SUN} \doteq 0.0092$ rad). This excess of instrumental acceptance
widths is sufficient to guarantee full-disk response even for observations made with
intended or inadvertent offset angles greater than those actually used in all geo-
physical routine turnons of the EUVS experiment on all of these AE satellites. The
center of the instrumentally viewed field of solar EUV source is then of course
identical with the center of the solar disk, and the algorithms developed in Section
A1 are relevant only for the assessment of the spread of zenith angles ($\Delta\chi$) and
remotely probing heights (Δh_Q) associated with the spread of solar source-point
coordinates, $0 \leq |\epsilon| \leq 0.0046$ and $0 \leq |\gamma| \leq 0.0046$, regardless of SPS target
offsets if any (up to at least 2-3 offset steps as illustrated in Figure A1) and regard-
less of individual monochromator misalignment angles of values even exceeding the
worst actual cases of $\epsilon_{MN} \neq 0$ and $\gamma_{MN} \neq 0$ in the AE-C instrument.

For these full-disk MN's the expression (Eq. A14) for Δh_Q is, therefore, replaced by the simple relation

$$\Delta h_Q \doteq 0.0092 \, P \cos (180° - \chi_o); \, \Delta h_Q \, (\chi \leq 90°) = 0 ,\tag{A15}$$

where $P \cos (180° - \chi_o)$ is the distance of the remote-probing point from the satellite, and the total spread of zenith angles associated with all source points on the solar disk becomes

$$\Delta \chi \doteq 0.0092 \, \text{rad}\tag{A16}$$

for all values of the solar zenith angle associated with the ray from the center of the solar disk (χ_o).